Observation of Gap Opening in 1T′ Phase MoS₂ Nanocrystals

Hai Xu,[†,§,○] Dong Han,[‡,○] Yang Bao,[†] Fang Cheng,[†] Zijing Ding,[§] Sherman J. R. Tan,[†,∥] and Kian Ping Loh[*,†,§]

[†]Department of Chemistry, National University of Singapore, 3 Science Drive 3 117543, Singapore
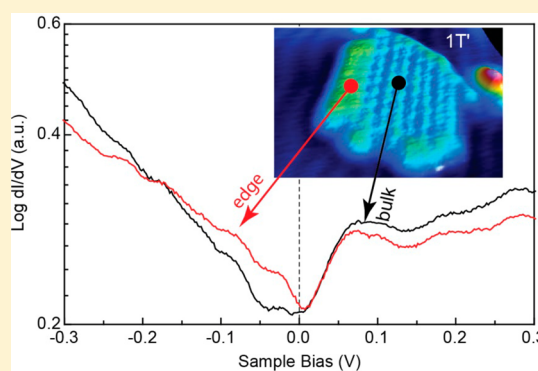
[‡]State Key Laboratory of Luminescence and Applications, Changchun Institute of Optics Fine Mechanics and Physics, Chinese Academy of Sciences, Changchun 130033, People's Republic of China

[§]Centre for Advanced 2D Materials and Graphene Research Centre, National University of Singapore 117546, Singapore

[∥]NUS Graduate School for Integrative Sciences and Engineering, National University of Singapore 117456, Singapore

ABSTRACT: Two-dimensional (2D) transition metal dichalcogenides (TMDs) manifest in various polymorphs, which deliver different electronic properties; the most prominent among them include the semiconducting 2H phase and metallic 1T (or distorted 1T′ phase) phase. Alkali metal intercalation or interface strain has been used to induce semiconductor-to-metal transition in a monolayer MoS₂ sheet, leading to exotic quantum states or improved performance in catalysis. However, the direct growth of 1T or 1T′ phase MoS₂ is challenging due to its metastability. Here, we report MBE growth of isolated 1T′ and 2H MoS₂ nanocrystals on a Au substrate; these nanocrystals can be differentiated unambiguously by their electronic states using scanning tunneling microscopy (STM) and scanning tunneling spectroscopy (STS). By studying the initial stages of nucleation during molecular beam epitaxy (MBE) of MoS₂, we could identify atomic clusters (30−50 atoms) with intralayer stacking corresponding to 1T′ and 2H separately, which suggests a deterministic growth mechanism from initial nuclei. Furthermore, a topological insulator type behavior was observed for the 1T′ MoS₂ crystals, where an energy gap opening of 80 meV was measured by STS in the basal plane at 5 K, with the edge of the nanocrystals remaining metallic.

KEYWORDS: Two-dimensional materials, MoS₂, phase transition, quantum spin Hall effect (QSH), scanning tunneling microscopy (STM)

Two-dimensional (2D) transition metal dichalcogenides (TMDs) such as MoS₂ are a versatile platform for optoelectronic devices because of their thickness-tunable properties, which include strong light−matter interactions, valley degrees of freedom, and direct band gaps at the monolayer limit.[1−5] Structural transition from trigonal prismatic (2H) to octahedral (1T) M−X (M = Mo, Ti, W, Ta; X = S, Se, Te) coordination can be induced by a change in the d orbital electron density; these different polymorphs deliver a diverse range of properties, which can be exploited for different applications.[1−4] The 1T phase, however, is not stable and distorts to form the 1T′ phase, which can be considered as a charge density wave state of 1T-MoS₂ due to the Peierls instability.[5,6] The 1T′ phase was often ambiguously assigned as 1T in early literature.[6−8] Recently, the 1T′ phase has attracted considerable interests because of its topological properties, whereby Weyl semimetallicity and quantum spin Hall effects (QSH) have been observed in epitaxially grown 1T′-MoTe₂ and -WTe₂.[1,2,9,10] Particularly, an intrinsic band inversion between chalcogenide-p and metal-d arising from the structural distortion in 2D 1T′ phase TMCs opens a larger band gap than conversional 3D QSH insulators. The 2H-to-1T/1T′ phase transition in MoS₂ was previously triggered by alkali metal

intercalation (e.g., Li and K)[11−13] or metal atom substitutional doping.[14,15] Besides the difficulty in handling, the intercalation process can degrade the crystallinity of the host lattice and deteriorate properties. For example, a lithiated and exfoliated MoS₂ sheet was reported to be converted to a nanocrystalline phase.[7,11,16] In view of that, a bottom up synthesis approach is desirable, the small energy barrier (<0.4 eV per unit cell) between the 2H and 1T phases in group VI TMDs with Te- or Se-based chalcogens allows the direct synthesis of these compounds.[17,18] However, the growth of sulfur-based 1T or 1T′ phase MoS₂, which have much larger 2H/1T phase barriers (>0.5 eV per unit cell), is more challenging. Both theory and experiments suggest that defects, impurities, and mechanical stress can stabilize the 1T/1T′ phase.[14,19,20] One less explored option is by changing the chemical potential or temperature during the growth, since this should affect the relative stability of the 2H and 1T/1T′ phases. To elucidate the electronic structure of the 1T′ phase, it is essential that the

1T′ phase is isolated from the 1H. (We call 2H as 1H to denote a monolayer structure.)

Herein, we have performed MBE growth of 1H and 1T′ phase MoS$_2$ nanosized islands on Au (111). Taking advantage of the precision in the growth fluxes, we investigated how changing the relative ratio of S and Mo affects the polymorph evolution. At the early nucleation stage, the isolated 1T/1T′ or 1H-MoS$_2$ nanoclusters (30−50 atoms) can be clearly distinguished by scanning tunneling microscopy (STM), suggesting that the majority of the 1T/1T′ and 1H nanocrystals grow independently, although an abrupt homo-junction can be occasionally observed between the two. The 1H phase has a much larger STS-determined gap of 1.6 eV compared to the metallic 1T/1T′ phase, in agreement with their respective semiconductor and semimetallic character. Importantly, a gap opening of 80 meV was observed for the 1T′ nanocrystal at cryogenic temperatures, which agrees with quantum spin Hall type characteristics predicted for the 1T′ phase.

Due to its chemical inertness and small lattice mismatch with MoS$_2$, Au (111) serves as a good template for the synthesis of MoS$_2$ of one unit cell thickness (monolayer).[14−17] The characteristic herringbone reconstruction of the Au (111) surface generates periodic lattice dislocations (elbow sites), which provides nucleation sites for MBE-deposited molybde-num (Mo) clusters. MoS$_2$ nanoclusters or islands were grown by directly depositing Mo clusters in a sulfur-rich environment (H$_2$S pressure ∼ 1×10^{-6} mbar) and subsequently sulfidation of the predeposited Mo clusters in a sulfur-rich environment. At a lower growth temperature of ∼500 °C, 1H phase MoS$_2$ islands with characteristic Moiré patterns were exclusively grown on Au (111) (Figure 1c). When the temperature was increased to 600 °C and the Mo/S ratio in the growth flux was kept the same, two types of MoS$_2$ monolayer (ML) nanoislands with different contrasts were observed (Figure 1a,b). The islands with the bright STM contrast are tentatively identified as the 1T phase MoS$_2$, and the dark islands are tentatively identified as the 1H phase (labeled in Figure 1b,c, respectively). To confirm the phase assignment, we have performed X-ray photoelectron spectroscopy (XPS) on films grown with purely 1H phase samples or 1T phase samples (see Figure 3c). It was observed that the Mo 3d$_{5/2}$ in the bright islands has a binding energy of 228.2 eV, which is chemically downshifted from that of 1H-MoS$_2$ at 229.4 eV (Figure 1c); the chemical shift agrees with what was reported for the 1T phase.[11] The 1H phase of MoS$_2$ has a d^2 electronic configuration with Mo in the +4 oxidation state. The addition of electrons destabilizes the 1H phase with respect to the 1T′ phase, in which the Mo is reduced from the +4 oxidation state to the +3 oxidation state, leading to a chemical downshift of the Mo core level XPS peak.[21−23] In our work, we hypothesize that a gold substrate serves as an electron reservoir,[24] whose doping of MoS$_2$ leads to a chemical downshift of the Mo core level XPS peak (see the later discussion).

An interesting question arises as at what stage of the growth process did the 1T structure develop; did the 1T island grow from a nucleating cluster or nucleate from defects in a 1H island? To answer this question, we quenched the growth process after 5 min of growth and studied the distribution of small-sized MoS$_2$ clusters consisting of about 30−50 Mo and S atoms. Figure 2a depicts two distinct MoS$_2$ nanoclusters formed at the early nucleation stage. The atomic structures of 1H- and 1T-MoS$_2$, as well as the structural transition from 1H
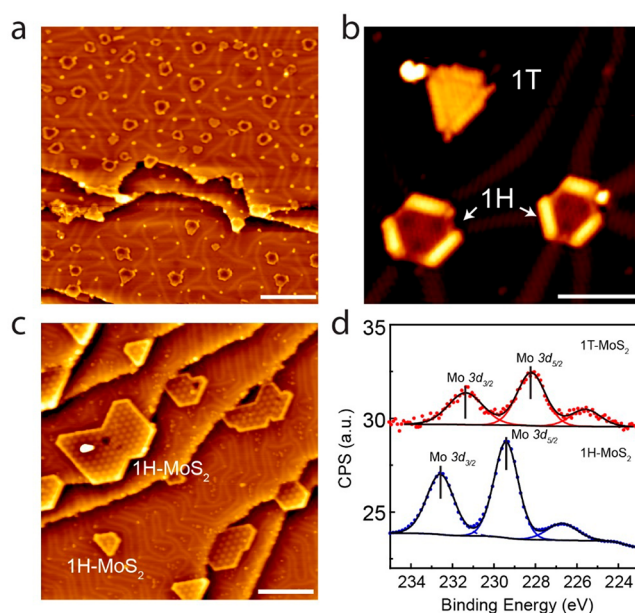

Figure 1. Growth of mixed 1H and 1T phase MoS$_2$ on Au (111). (a) STM image of mixed-phase MoS$_2$ islands on Au (111) ($V_s = -1.2$ V, $I_t = 800$ pA), grown by e-beam deposition of Mo (8 min) onto Au (111) in an atmosphere of 1×10^{-6} mbar H$_2$S at 600 °C, and postannealing in H$_2$S for 40 min. (b) Magnified STM image of 1T- and 1H-MoS$_2$ islands ($V_s = -1.0$ V, $I_t = 500$ pA). (c) STM image showing the large ML 1H-MoS$_2$ islands by predepositing Mo (15 min) on the Au surface ($V_s = -1.2$ V, $I_t = 800$ pA), followed by annealing at ∼500 °C in an atmosphere of 1×10^{-6} mbar H$_2$S for 2 h, then slow cooling to RT (2 h). Scale bar: (a,d) 20 nm, (b) 5 nm. (d) X-ray photoelectron spectrum of pure 1T-MoS$_2$ synthesized on the Au surface. Spectrum shows the Mo 3d core level peaks. Spectrum of 1H-MoS$_2$ on Au is included as a comparison.

to 1T mediated by the gliding of the sulfur atomic plane over the Mo plane, are schematically illustrated in Figure 2b. From left to right, Figure 2c shows the proposed atomic structure of the 1H-MoS$_2$ nanocluster ($N = 4$), its density functional theory (DFT)-simulated STM image and the corresponding exper-imental STM image. Here, the size of the nanocluster is defined in terms of the number of Mo atoms (N) at the edge of MoS$_2$.[25] Previous studies reported that the edge termination of 1H phase MoS$_2$ is size-dependent, with small clusters ($N \leq 6$) terminated by S edges and large clusters terminated by Mo edges.[25] The DFT-simulated image of the proposed $N = 4$ S edge-terminated 1H cluster reproduces the experimental STM image with bright center protrusions and faint edges.[25−27] This is distinguished from the larger clusters and islands of the 1H phase (Figure 1b), which are terminated by zigzag Mo edges that show bright brim contrast instead. The edge termination of 1T phase MoS$_2$ has not been studied before, and hence several possible structures were proposed to fit our observed STM image, among which the $N = 4$ 1T cluster with sulfur-terminated edges (see Figure 2d, left) is most probable. Middle panel of Figure 2d shows the DFT-simulated STM image based on the proposed 1T-cluster structure. The agreement between experimental and simulated STM images provides compelling evidence for the existence of 1T-MoS$_2$ clusters at the early nucleation stage. This suggests that a small MoS$_2$ cluster fluctuates as a single coherent unit and can transform into either the 1H or 1T phase depending on their relative thermodynamic stabilities during growth. However, previous
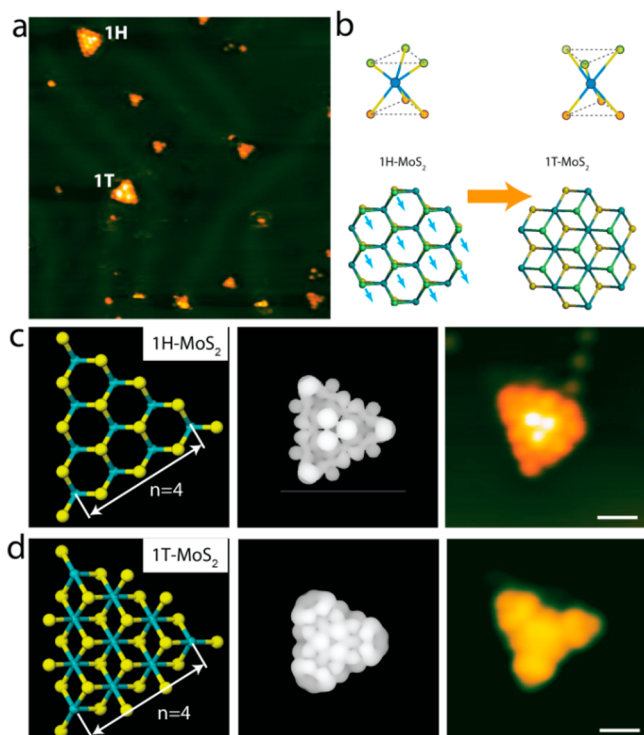
Figure 2. Nucleation of 1H and 1T phase MoS$_2$ clusters on Au. (a) Large scale STM image of the early stage nucleation clusters on the Au surface (V_s = −0.5 V, I_t = 800 pA). (b) Schematic illustration of prismatic and octahedral units of MoS$_2$ and the sliding transformation from 1H to 1T structure. (c) Left to right: proposed structure of the 1H-MoS$_2$ cluster and its DFT-simulated STM image and experimental STM image, respectively; Scale bar: 0.5 nm. (d) Left to right: proposed structure of the 1T-MoS$_2$ cluster and its DFT-simulated STM image and experimental STM image, respectively. Scale bar: 0.5 nm. (c,d) Scanning parameters: V_s = −0.1 V, I_t = 1 nA.

experiments and DFT calculations suggest that the 1T phase is energetically unfavorable and Fermi surface nesting drives its spontaneous conversion to the 1T′ phase.[2,7,8,12,16] So we assign the bright triangular 1T phase MoS$_2$ nanoislands as 1T′ phase; this assignment is also supported by our high-resolution atomic STM images shown later.

In the 1H−1T′ two-phase MoS$_2$ system, the 1H−1T′ phase transition can be triggered by charge transfer from extrinsic impurity atoms or intrinsic chalcogen vacancies.[8,12,14,24] The Au substrate can be regarded as an electron reservoir, whose doping of MoS$_2$ will create greater Fermi surface nesting and stabilize the 1T′ phase.[24] In our experiments, we found that quenching the growth rapidly (fast cooling) allows a greater number of 1T′ phase MoS$_2$ islands to be observed as compared to slow cooling (see histogram of the 1T′ and 1H distribution in Figure 3a,b), suggesting that some 1T′ may have converted to 1H during the slow cooling process. We hypothesize that both 1H and 1T′ nucleate separately during high-temperature growth, but during the cooling process, the metastable 1T′ converts to 1H. Therefore, rapid cooling allows MoS$_2$ domains to be kinetically quenched at the metastable 1T′ phase, whereby thermal energies are insufficient for the islands to overcome the activation barrier for the 1T′-to-1H phase transition. Interestingly, decreasing the chemical potential of S was found to promote the selective growth of the 1T′ phase (Figure 3c), which provides evidence that the energetics between these two phases are chemical potential-dependent.
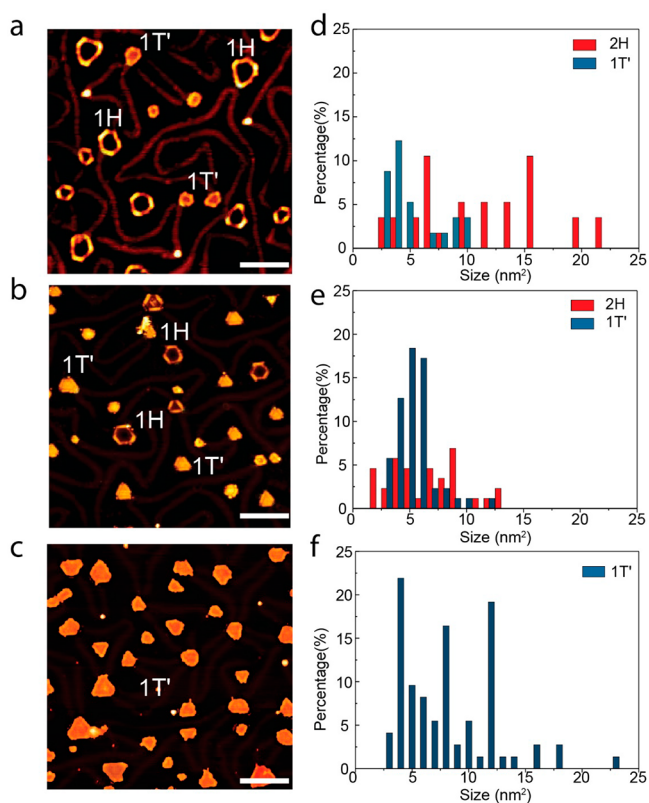

Figure 3. Statistical distribution of 1H- and 1T′-MoS$_2$ islands grown at different conditions. STM images of 1H- and 1T′-MoS$_2$ islands grown on the Au (111) surface. (a) After 15 min of Mo deposition, the sample was annealed at 600 °C in a H$_2$S environment for 40 min (H$_2$S partial pressure of 1.0 × 10^{-6} mbar) and slow cooling to room temperature (RT) in 2 h. (b) same growth as panel a, with a fast cooling time to RT of 45 min. (c) After 15 min of Mo deposition, the sample was annealed at 600 °C in a H$_2$S environment of 40 min (H$_2$S partial pressure of 5.0 × 10^{-7} mbar) and slow cooling time to RT (2 h). Panels d−f are the corresponding histograms for panels a−c. Scale bar: 10 nm. Scanning parameters: V_s = −1.0 V, I_t = 800 pA.

We hypothesize that the formation energy of 1T′ phase MoS$_2$ is lowered at a decrease chemical potential of S, due perhaps to relative stability of the edge reconstruction.[28,29]

To shed light on the atomic and electronic structures of the two phases, we performed high-resolution STM and STS studies on similarly sized 1H- and 1T′-MoS$_2$ nanoislands at LN$_2$ (77.8 K). As shown in Figure 4a, a sharp contrast in the tunneling conductance exists between the edges and center of the 1H-MoS$_2$ islands. This is explained by the semiconducting character of the center, which is typical of the basal plane of 1H-MoS$_2$, and the presence of metallic edge states localized at the zigzag Mo edges.[25−27] On the other hand, with the same imaging parameters, the tunneling conductance is uniform throughout the 1T′-MoS$_2$ island, as shown in Figure 4c. The brighter contrast in the center of the 1T′ phase island implies a higher tunneling conductance than that of the 1H phase, which is consistent with the prediction that the 1T′ phase is semimetallic and that the 1H phase is semiconducting.[8,30] The different electronic properties between 1H and 1T′ are further highlighted by the dI/dV spectra (Figure 4b). The dI/dV spectrum recorded at the center of the 1H islands shows a distinct peak located at 0.98 ± 0.02 eV, assignable to the conduction band (CB) edge of MoS$_2$, and another distinct peak assignable to the valence band edge appears at −1.0 ±
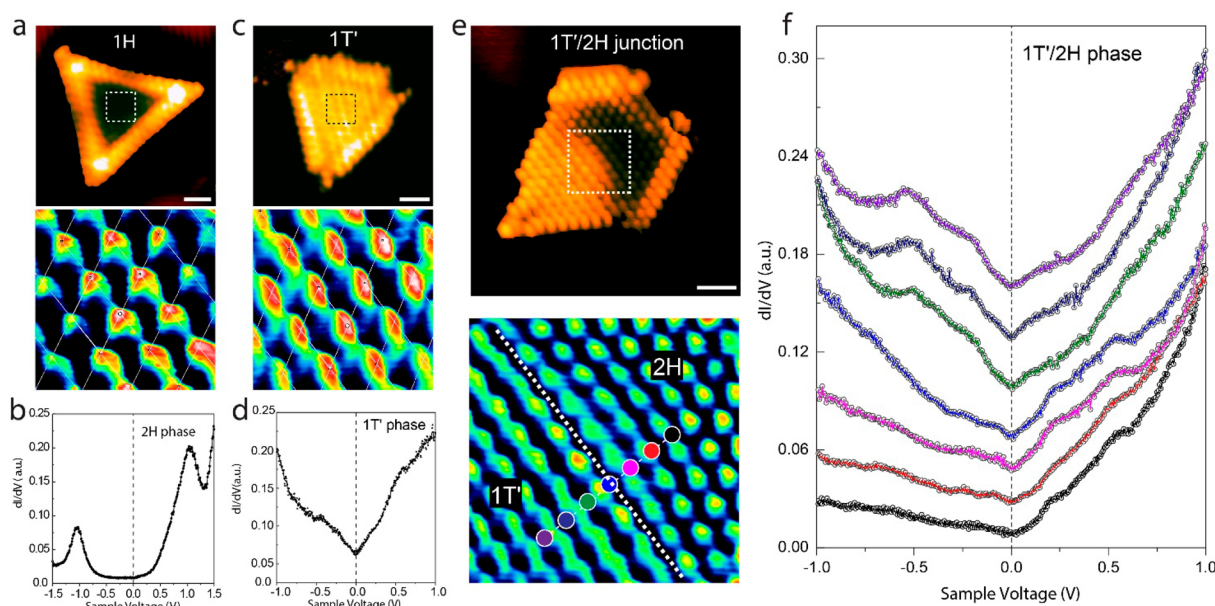
Figure 4. Atomic and electronic structure of 1H/1T′-MoS$_2$ nanocrystals. (a,b) STM image and STS of the 1H-MoS$_2$ nanocrystals. (c,d) STM image and STS of the 1T-MoS$_2$ nanocrystals. (e) STM image of a MoS$_2$ island with merged 1T′−1H domains. (f) A set of spatially resolved STS spectra acquired across the 1T′−1H junction acquired at LN$_2$ (77.8 K). The acquired point of each curve is marked by the corresponding colored dot in panel e. Scale bar: 1 nm. Scanning parameters: V_s = −0.6 V, I_t = 1 nA.

0.02 eV; this yields a band gap of 1.6 eV, which is comparable with band gaps determined from STM measurements on MoS$_2$/Au systems,[31−33] but smaller than the bulk band gap of MoS$_2$ (1.84 eV). The reduced band gap may be due to interface strains and charge screening by the Au substrate.[31,32] In contrast, gapless "V-shaped" dI/dV spectra centered at the Femi level (E_f) were observed for 1T′-MoS$_2$ islands (Figure 4d). In addition to isolated islands, we have also observed 1H/1T′-MoS$_2$ lateral homojunctions. Figure 4e shows the STM image of one such junction with seamlessly merged 1T′ and 1H domains (no lattice reconstruction at the domain boundary). The junction is abrupt and a sharp semimetallic−semiconductor transition is observed across the 1T′/1H homojunction (Figure 4f).

Atomic structures of the surface of 1H and 1T′ islands are shown in the lower panel of Figure 4a,c, respectively, in which the atomic protrusions reflect the surface sulfur atom positions. The measured protrusion periodicity of the 1T′ phase is about 0.33 nm, which is larger than that of 0.31 nm measured in the 1H phase. It verified that the lattice of the 1T′ phase is distorted. Moreover, the elongated atomic protrusions in the 1T′-MoS$_2$ islands appear more chain-like compared to that in the 1H islands, although we are not able to resolve a clear 2 × 1 reconstruction, which is expected for the 1T′ phase.

Interestingly, we observed a gap opening at E_f in the 1T′ islands when the sample was cooled to 4.5 K. In Figure 5a, the dI/dV spectra taken at the center of 1T′ islands show a small gap at E_f instead of the sharp V shape observed at 77.8 K. The zoom-in dI/dV curves taken at the center and edge of 1T′ islands, respectively, are shown in Figure 5b, where an energy gap of 75 ± 5 meV opens at the center. STS reveals that the edge maintains its metallic behavior, which might be due to the one-dimensional (1D) nature of the edge states. Figure 5c shows a series of STS taken from edge to center along the mark line in the top panel, which clearly reveals that the conductance is only localized at the edge regions.
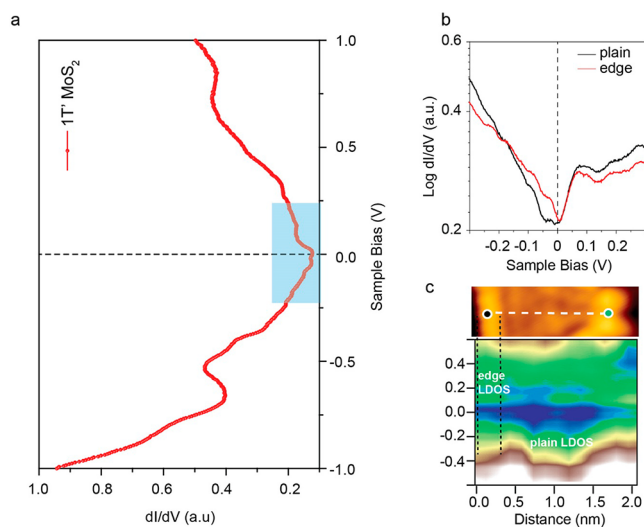

Figure 5. Electronic structure of 1T′-MoS$_2$ nanocrystals at 4.5 K. (a) STS taken at the bulk of the 1T′-MoS$_2$ nanocrystals. (b) Zoom-in STS of the 1T′-MoS$_2$ nanocrystals taken at the edge and bulk. (c) STM image and a set of spatially resolved STS spectra acquired from the edge to bulk along the dashed line shown in the STM image at the top of panel c. Scanning parameters: V_s = −0.6 V, I_t = 500 A.

The gap opening observed for the basal plane regions of the 1T′-MoS$_2$ islands in this work echoes the gap opening observed for monolayer 1T′-WTe$_2$ islands and few layers 1T′-MoTe$_2$ film,[9,10] which were explained by the breaking of the band degeneracy by spin−orbit coupling (SOC) effects in the distorted 1T′ phase; these give rise to topologically nontrivial quantum states as the metallic edge states are protected by time reversal symmetry, while a band gap opens in the bulk. To see if a gap opening occurs for the 1T′-MoS$_2$ phase due to SOC effects, we have performed density functional theory (DFT)[34,35] calculations using the VASP codes.[36] The generalized gradient approximation (GGA)[37]
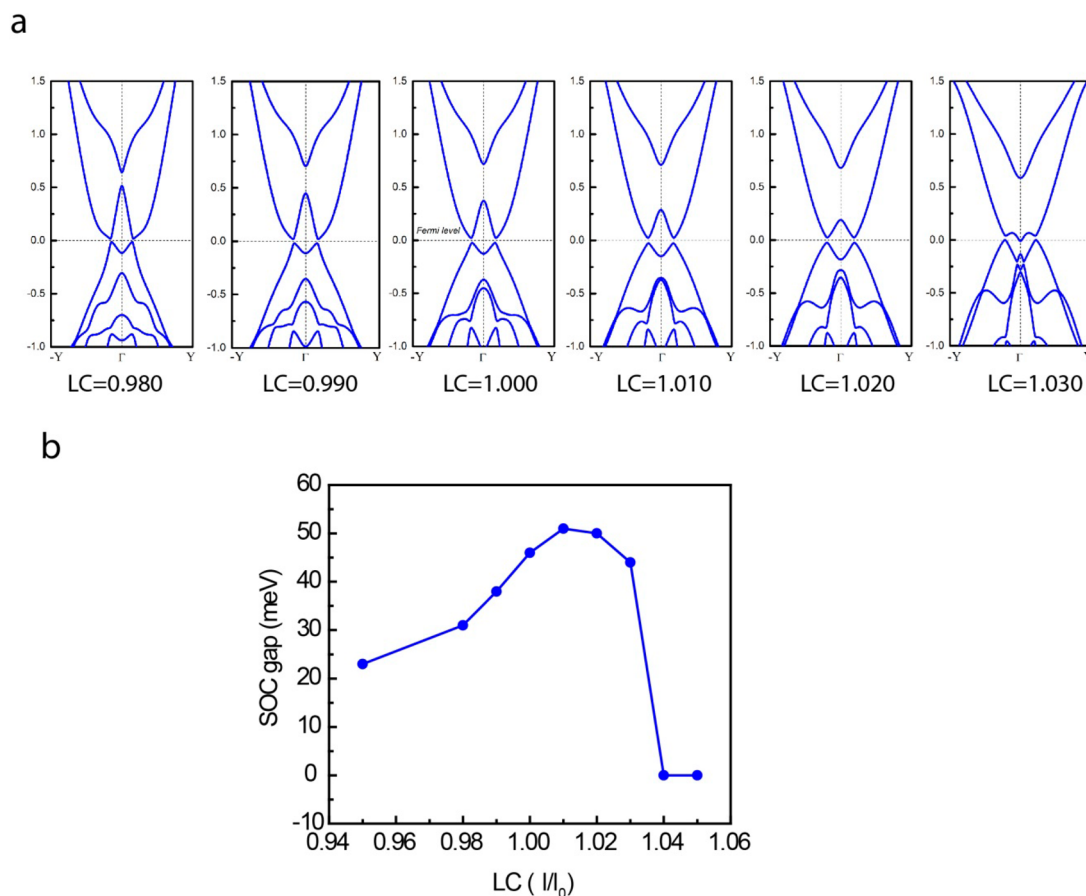
a

LC=0.980   LC=0.990   LC=1.000   LC=1.010   LC=1.020   LC=1.030

b

Figure 6. DFT calculations of the band structure of monolayer 1T′-MoS$_2$ as a function of strain. (a) The band gap of monolayer 1T′-MoS$_2$ from $-Y$ to Γ to Y in Brillouin zone changes with the variation in-plane lattice l, where $l = 1.000$ is the equilibrium lattice parameter l_0. The Fermi level is set to zero. (b) Effect of biaxial strain on fundamental gap (E_g).

with the Perdew−Burke−Ernzerhof[38] functional and projector augmented wave basis[39] were employed. The cutoff energy and Monkhorst−Pack k-point mesh grid are 400 eV and $7 \times 13 \times 1$, respectively. The primitive cell of 1T′ phase MoS$_2$ is used with the in-plane lattice $a = 5.716$ Å and $b = 3.181$ Å. The out-plane lattice c is set to 20 Å, in order to avoid interactions between periodic images. The atomic geometries in the primitive cell were fully optimized until the Hellman−Feynman forces on each atom were smaller than 0.014 eV/Å. For the calculations of band structures and density of states, SOC is included. In the absence of SOC, because of the symmetry breaking in the lattice of 1T′, the d$_{z_2}$ orbital of Mo atoms is lowered below E_f, whereas the d$_{xz}$ orbital lifts in the opposite direction near the Γ(G) point, which results in the band crossing at E_f to form two Dirac cones centered at finite momenta on Y-Γ-Y in the 2D Brillouin zone (BZ). After including SOC, the bands further hybridize with each other and the degeneracies at the Dirac cones are lifted, producing a small gap of 46 meV. Since the monolayer 1T′ islands are grown on Au (111), where interface strain due to lattice mismatch may affect the electronic properties, we analyzed the calculated band structures of monolayer MoS$_2$ as a function of compressive or tensile strains as shown in Figure 6a. The calculations show a gap opening of 46 meV near the Γ(G) point in the Brillouin zone when the monolayer crystal is strain free. At 1−2% tensile strain, the gap can be enlarged to 51−50 meV, but larger tensile strain decreases the fundamental band relative to the Fermi level, closing the gap. Compressive strain

of 1−2% reduces the gap significantly to between 38 and 31 meV. In view of this, the STM-measured gap of 75 meV should not be due to strain effects. One possibility is that the enhanced electron correlation energy in a nanocrystal contributes to the larger gap opening than that predicted by theory. The synthesized monolayer MoS$_2$ islands are the size of quantum dots, and thus in-plane quantum confinement effects may further modulate the electronic properties on top of the SOC effects.

In summary, we have demonstrated the MBE growth of individual 1H- and 1T′-MoS$_2$ nanocrystals on Au (111). At the initial nucleation stage, nanoclusters of 30−50 atoms size already showed distinct intralayer stacking order that allows them to be differentiated as 1T or 1H polymorph. From these nanoclusters, the deterministic formation of 1T′ or 1H phase MoS$_2$ nanocrystals occurs. Rapid quenching of the growth allows the 1T′ phase to be isolated. At a high growth temperature and low sulfur chemical potential, 1T′-MoS$_2$ can be selectively grown. STS measurements at 4.5 K reveal that a gap of 75 ± 5 meV opens in the basal plane of 1T′ phase MoS$_2$ nanocrystals, these have been explained by our DFT calculations to be related to the SOC-lifting of band degeneracy. Finally, our growth studies suggest that it should be possible to make nanocrystalline 1T′ films if the nucleation density can be increased.

◼ AUTHOR INFORMATION

Corresponding Author

*E-mail: chmlohkp@nus.edu.sg. Phone: +65-65164402.

ORCID 🔘

Fang Cheng: 0000-0003-1645-4237

Sherman J. R. Tan: 0000-0003-1591-3497

Kian Ping Loh: 0000-0002-1491-743X

Author Contributions

○H.X. and D.H. contributed equally to this work.

Notes

The authors declare no competing financial interest.

◼ REFERENCES

(1) Sun, Y.; Wu, S.-C.; Ali, M. N.; Felser, C.; Yan, B. *Phys. Rev. B: Condens. Matter Mater. Phys.* **2015**, *92*, 161107.

(2) Qian, X.; Liu, J.; Fu, L.; Li, J. *Science* **2014**, *346*, 1344.

(3) Acerce, M.; Voiry, D.; Chhowalla, M. *Nat. Nanotechnol.* **2015**, *10*, 313.

(4) Acerce, M.; Akdoğan, E. K.; Chhowalla, M. *Nature* **2017**, *549*, 370.

(5) Chen, X.; Chen, Z.; Li, J. *Chin. Sci. Bull.* **2013**, *58*, 1632.

(6) Rocquefelte, X.; Boucher, F.; Gressier, P.; Ouvrard, G.; Blaha, P.; Schwarz, K. *Phys. Rev. B: Condens. Matter Mater. Phys.* **2000**, *62*, 2397.

(7) Wypych, F.; Schollhorn, R. *J. Chem. Soc., Chem. Commun.* **1992**, 1386.

(8) Hu, T.; Li, R.; Dong, J. *J. Chem. Phys.* **2013**, *139*, 174702.

(9) Keum, D. H.; Cho, S.; Kim, J. H.; Choe, D.-H.; Sung, H.-J.; Kan, M.; Kang, H.; Hwang, J.-Y.; et al. *Nat. Phys.* **2015**, *11*, 482.

(10) Tang, S.; Zhang, C.; Wong, D.; Pedramrazi, Z.; Tsai, H.-Z.; Jia, C.; Moritz, B.; Claassen, M.; et al. *Nat. Phys.* **2017**, *13*, 683.

(11) Yang, D.; Sandoval, S. J.; Divigalpitiya, W. M. R.; Irwin, J. C.; Frindt, R. F. *Phys. Rev. B: Condens. Matter Mater. Phys.* **1991**, *43*, 12053.

(12) Eda, G.; Fujita, T.; Yamaguchi, H.; Voiry, D.; Chen, M.; Chhowalla, M. *ACS Nano* **2012**, *6*, 7311.

(13) Chhowalla, M.; Shin, H. S.; Eda, G.; Li, L.-J.; Loh, K. P.; Zhang, H. *Nat. Chem.* **2013**, *5*, 263.

(14) Enyashin, A. N.; Yadgarov, L.; Houben, L.; Popov, I.; Weidenbach, M.; Tenne, R.; Bar-Sadan, M.; Seifert, G. *J. Phys. Chem. C* **2011**, *115*, 24586.

(15) Lin, Y.-C.; Dumcenco, D. O.; Komsa, H.-P.; Niimi, Y.; Krasheninnikov, A. V.; Huang, Y.-S.; Suenaga, K. *Adv. Mater.* **2014**, *26*, 2857.

(16) Wypych, F.; Weber, T.; Prins, R. *Chem. Mater.* **1998**, *10*, 723.

(17) Duerloo, K.-A. N.; Li, Y.; Reed, E. J. *Nat. Commun.* **2014**, *5*, 4214.

(18) Zhou, Y.; Reed, E. J. *J. Phys. Chem. C* **2015**, *119*, 21674.

(19) Dolui, K.; Rungger, I.; Das Pemmaraju, C.; Sanvito, S. *Phys. Rev. B: Condens. Matter Mater. Phys.* **2013**, *88*, 075420.

(20) Cai, L.; He, J.; Liu, Q.; Yao, T.; Chen, L.; Yan, W.; Hu, F.; Jiang, Y.; et al. *J. Am. Chem. Soc.* **2015**, *137*, 2622.

(21) Kochat, V.; Apte, A.; Hachtel, J. A.; Kumazoe, H.; Krishnamoorthy, A.; Susarla, S.; Idrobo, J. C.; Shimojo, F.; et al. *Adv. Mater.* **2017**, *29*, 1703754.

(22) Tan, S. J. R.; Abdelwahab, I.; Ding, Z.; Zhao, X.; Yang, T.; Loke, G. Z. J.; Lin, H.; Verzhbitskiy, I.; et al. *J. Am. Chem. Soc.* **2017**, *139*, 2504.

(23) Yu, Y.; Nam, G.-H.; He, Q.; Wu, X.-J.; Zhang, K.; Yang, Z.; Chen, J.; Ma, Q.; et al. *Nat. Chem.* **2018**, *10*, 638.

(24) Kang, Y.; Najmaei, S.; Liu, Z.; Bao, Y.; Wang, Y.; Zhu, X.; Halas, N. J.; Nordlander, P.; et al. *Adv. Mater.* **2014**, *26*, 6467.

(25) Lauritsen, J. V.; Kibsgaard, J.; Helveg, S.; Topsoe, H.; Clausen, B. S.; Laegsgaard, E.; Besenbacher, F. *Nat. Nanotechnol.* **2007**, *2*, 53.

(26) Bollinger, M. V.; Lauritsen, J. V.; Jacobsen, K. W.; Nøtrskov, J. K.; Helveg, S.; Besenbacher, F. *Phys. Rev. Lett.* **2001**, *87*, 196803.

(27) Bollinger, M. V.; Jacobsen, K. W.; Nørskov, J. K. *Phys. Rev. B: Condens. Matter Mater. Phys.* **2003**, *67*, 085410.

(28) Cao, D.; Shen, T.; Liang, P.; Chen, X.; Shu, H. *J. Phys. Chem. C* **2015**, *119*, 4294.

(29) Schweiger, H.; Raybaud, P.; Kresse, G.; Toulhoat, H. *J. Catal.* **2002**, *207*, 76.

(30) Mak, K. F.; Lee, C.; Hone, J.; Shan, J.; Heinz, T. F. *Phys. Rev. Lett.* **2010**, *105*, 136805.

(31) Sorensen, S. G.; Fuchtbauer, H. G.; Tuxen, A. K.; Walton, A. S.; Lauritsen, J. V. *ACS Nano* **2014**, *8*, 6788.

(32) Bruix, A.; Miwa, J. A.; Hauptmann, N.; Wegner, D.; Ulstrup, S.; Grønborg, S. S.; Sanders, C. E.; Dendzik, M.; et al. *Phys. Rev. B: Condens. Matter Mater. Phys.* **2016**, *93*, 165422.

(33) Xu, H.; Ding, Z.; Nai, C. T.; Bao, Y.; Cheng, F.; Tan, S. J. R.; Loh, K. P. *Adv. Funct. Mater.* **2017**, *27*, 1603887.

(34) Hohenberg, P.; Kohn, W. *Phys. Rev.* **1964**, *136*, B864.

(35) Kohn, W.; Sham, L. J. *Phys. Rev.* **1965**, *140*, A1133.

(36) Kresse, G.; Furthmüller, J. *Comput. Mater. Sci.* **1996**, *6*, 15.

(37) Perdew, J. P.; Yue, W. *Phys. Rev. B: Condens. Matter Mater. Phys.* **1986**, *33*, 8800.

(38) Perdew, J. P.; Burke, K.; Ernzerhof, M. *Phys. Rev. Lett.* **1996**, *77*, 3865.

(39) Blöchl, P. E. *Phys. Rev. B: Condens. Matter Mater. Phys.* **1994**, *50*, 17953.